Coulomb effects in open quantum dots within the random-phase approximation

V. Moldoveanu[1] and B. Tanatar[2]
[1]*National Institute of Materials Physics, P.O. Box MG-7, 077125 Bucharest-Magurele, Romania*
[2]*Department of Physics, Bilkent University, Bilkent, 06800 Ankara, Turkey*
(Received 26 October 2007; revised manuscript received 7 April 2008; published 2 May 2008)

The effect of electron-electron interactions on coherent transport in quantum dot systems is theoretically investigated by adapting the well-known random-phase approximation (RPA) to the nonequilibrium Green–Keldysh formalism for open mesoscopic systems. The contour-ordered polarization operator is computed in terms of the Green functions of the noninteracting system. We apply the proposed RPA-Keldysh scheme for studying Coulomb-modified Fano lines and dephasing effects in interferometers with side-coupled many-level dots. Our method allows us to treat on equal footing the decoherence induced by the intradot interaction and that by the Coulomb coupling to a nearby system. In the case of a single interferometer, we show that the intradot Coulomb interaction leads to a reduction of the Fano line amplitude. From the analysis of the interaction self-energy, it follows that this effect originates in inelastic scattering processes in which electron-hole pairs are involved. The interplay between the interdot and the intradot interactions in decoherence is discussed for two nearby identical T-shaped interferometers. We also show that the intradot interaction does not prevent the observation of controlled dephasing due to a nearby charge detector, as long as the latter is subjected to a sufficiently large bias.

DOI: 10.1103/PhysRevB.77.195302 PACS number(s): 73.23.Hk, 85.35.Ds, 85.35.Be, 73.21.La

I. INTRODUCTION

Understanding the role of Coulomb interactions in transport phenomena at nanoscale has become an important task for an accurate description of the underlying physics, especially in the context of mesoscopic interferometry[1] and semiconductor spintronics.[2] The reason is twofold. On one hand, the electron-electron interactions in highly confined systems such as quantum dot arrays are responsible for nontrivial effects that are appealing from the applications point of view (Coulomb blockade,[3–6] Kondo correlated transport,[7] charge sensing,[8,9] etc.) On the other hand, it was theoretically predicted[10–12] that the coherent features of transport are damaged by the inelastic processes due to the Coulomb interaction of the system with its environment. This statement was confirmed later on in the experiment of Buks *et al.*[13] More precisely, it was reported that the Aharonov–Bohm oscillations in a ring with an embedded quantum dot are partially reduced when a quantum point constriction subjected to a finite bias is placed near the quantum dot. Since the properties of the constriction and of the dot are easily tunable, this decoherence process is also called controlled dephasing; it opened the way to indirect measurement techniques of quantum interference in mesoscopic systems. In contrast, the hyperfine interaction between the electronic and nuclear spins sets undesired limits for solid-state implementation of quantum computation algorithms.[14] The problem of decoherence induced by intradot interactions was theoretically addressed by Sivan *et al.*[15] and by Altshuler *et al.*[16]

Since electron-electron interactions are a built-in feature of semiconductor nanostructures, considerable experimental efforts nowadays are focused on designing suitable quantum dot-based devices allowing the "reading" of interference effects and the coherent manipulation of electrons while keeping the losses due to decoherence negligible. From the theoretical point of view, the description of quantum transport in interacting systems is not straightforward because one has to essentially deal with a many-body problem that leaves no room for an exact treatment except for very few simple models. One crucial point then is to choose appropriate approximation schemes for the Coulomb interaction in order to capture subtle effects that play an important role in coherent or incoherent transport.

In this work, we propose a treatment of the Coulomb interaction based on the random-phase approximation (RPA) and on the Keldysh formalism, which we find useful in the study of dephasing in mesoscopic interferometers. Both the RPA and the Keldysh approaches are well established formal tools that lead to important progress in the description of two-dimensional electron gas properties and of the mesoscopic transport phenomena. In spite of this fact, the possibility of combining them for studying open interacting systems driven by a finite bias has not been explored yet. In order to set the general context for our approach, we give in the following a brief account of the Keldysh formalism and of its main applications. The main idea behind the nonequilibrium Green's function formalism is to compute all relevant quantities of a system coupled to several biased leads by using the equilibrium state of the noninteracting disconnected system.[17–19] The coupling to the leads plays the role of the perturbation and is usually adiabatically switched. Then, a standard derivation leads to a closed formula for the current in terms of nonequilibrium Green functions. In the interacting case, the difficult and technical problem that remains to be solved is the calculation of these functions.

One approach is based on the equation-of-motion (EOM) method that was initiated by Zubarev[20] and is extensively used by many authors in the study of Anderson and Kondo Hamiltonians (see Refs. 21 and 22 and references therein). The usual strategy is to factorize the thermal averages of products of four creation (annihilation) operators in order to close the otherwise infinite chain of equations for higher-order Green functions (see, for example, Refs. 23 and 24).

One exactly solvable Fano–Kondo Hamiltonian within the EOM method is presented in a recent work.[25]

Another way to approximately compute interacting Green functions is to perform a perturbative expansion with respect to the interaction strength and to write down expressions for the first and second-order contributions to the interaction self-energy. This procedure successfully describes the controlled dephasing in mesoscopic interferometers Coulomb coupled to charge detectors.[26,27] This is because the second-order diagram for the interaction self-energy is the electron-hole bubble, which already takes into account inelastic processes that induce decoherence in the system. It should be mentioned that in this approach, a single-level quantum dot is considered and, therefore, the intradot interaction effect cannot be captured. König *et al.*[28] argued that a single-particle approximation oversimplifies the role of the interaction and therefore cannot capture decoherence effects due to intradot Coulomb repulsion. Clarifying the role of interdot interactions in decoherence as well as the interplay between intradot and interdot interactions in controlled dephasing constitutes another motivation for considering the RPA-Keldysh approach to steady-state transport in interacting quantum dot systems.

We mention that Faleev *et al.*[29] performed a self-consistent RPA calculation of the equilibrium Green functions and interaction self-energies for a homogeneous two-dimensional electron gas in the Kadanoff–Baym framework. Our approach is similar, the difference being that we consider *open* systems subjected to a finite bias and that the numerical simulations are done for lattice models. In a recent work, Wulf *et al.*[30] calculated the admittance of one-dimensional open systems subjected to an additional ac bias superimposed to the source-drain bias. The steady-state regime of the system (that is, in the absence of the ac bias) is described within the Landauer formalism and the random-phase approximation is used to estimate the density change induced by the ac bias. Here, we study steady-state transport and focus on decoherence effects due to electron-electron interactions. We present two applications that are relevant to the dephasing problem in mesoscopic interferometers. The first model system we consider is a many-level one-dimensional quantum dot side-coupled to a single channel lead (the so-called T-shaped interferometer).

These systems attracted considerable attention since the observation of the Fano interference in the experiment of Kobayashi *et al.*[31] Johnson *et al.*[9] also reported different transport regimes of a quantum dot coupled to a single conducting channel: pure Coulomb peaks and charge sensing effect at very weak coupling to the channel or Coulomb-modified Fano lines at moderate coupling. The charge sensing effect allows measurements of Coulomb blockade with noninvasive voltage probes and requires a theoretical description beyond the orthodox picture of the Coulomb blockade.[32,33]

The role of electron-electron interactions on the transport properties of side-coupled quantum dots has been theoretically investigated especially in the context of the Fano–Kondo effect.[34] Solving this problem requires nonperturbative techniques (such as the slave-boson mean-field theory or the renormalization group method) for dealing with the on-site (Hubbard) interaction at the quantum dot, which leads to the strongly correlated Kondo state.[35–37] Numerical or analytical results have been obtained for single-level quantum dots only. On the other hand, Orellana *et al.*[38] considered a one-dimensional side-coupled array of noninteracting quantum dots and found that the transport properties (resonances or antiresonances) depend on the number of sites in the array (odd or even). The conductance is computed by using a recursive formula for the retarded Green function. Nevertheless, to our best knowledge, no calculation of the Fano interference for interacting many-level side-coupled dots has been done yet.

The paper is organized as follows: In Sec. II, we describe the method in a rather general form, in the sense that we do not specialize to the tight-binding Hamiltonian of a given structure. All we assume is that the electron-electron interactions are present only in some central region and not in the leads, as it is usually done in the Keldysh formulation of electronic transport. The spin degrees of freedom and the Kondo problem are not considered in this work. For the role of spin-flip effects in dephasing, we refer to the works of König and Gefen[39] and of Silva and Levit.[40] In Sec. III, we show that the Fano interference is reduced when the Coulomb interactions inside the dot are taken into account. In the second half of Sec. III, we take two nearby T-shaped interferometers and investigate in detail their coherence properties in the presence of interdot and intradot interactions. The effect of a charge detector placed near the side-coupled quantum dot is also discussed. Finally, Sec. IV is devoted to conclusions.

II. FORMALISM

In any theoretical approach to interacting quantum transport, one starts with a formal tool to write down a formula for the current through the considered system, in terms of the interacting quantities. The explicit results are then obtained by using approximation schemes for the interaction effects. Here, we use the nonequilibrium Keldysh formalism for electronic transport and the random-phase approximation for the Coulomb interaction. In view of the numerical implementation, we shall work with tight-binding Hamiltonians. The system configuration is typical to the Keldysh approach: a central region (C) is coupled to noninteracting semi-infinite leads via a time-dependent switching $\chi(t)$. An adiabatic coupling is tacitly assumed in most of the theoretical calculations,[17,41] which means that $\chi(t)$ vanishes in the remote past, and the steady-state current is computed in the long-time limit. Actually, recent rigorous results show that the steady-state current does not depend on the way in which this coupling is achieved.[42] Transient current calculations within the Keldysh formalism for noninteracting dots that are suddenly coupled to biased leads were also performed recently.[43]

We use the index γ for the leads and $d_i^\dagger(d_i)$ is the pair of creation (annihilation) operators corresponding to the ith site of the lead. We also denote by $a_l^\dagger(a_l)$ the creation (annihilation) operators on the lth site of the lattice describing the central region. Then, the system Hamiltonian quite generally reads

$$H(t) = H_{\text{cen}} + H_{\text{leads}} + \chi(t)(H_{\text{tun}} + H_{\text{int}}),$$

$$H_{\text{cen}} = \sum_{l,m\in C} (\varepsilon_l \delta_{lm} + t_{lm}) a_l^\dagger a_m,$$

$$H_{\text{leads}} = t_L \sum_\gamma \sum_{<i,j>\in L_\gamma} d_i^\dagger d_j,$$

$$H_{\text{tun}} = \sum_{i\in L_\gamma} \sum_{l\in C} (V_{il}^\gamma d_i^\dagger a_l + \text{H.c.}),$$

$$H_{\text{int}} = \frac{U}{2} \sum_{l\neq m} \frac{\hat{n}_l \hat{n}_m}{|r_l - r_m|}. \tag{1}$$

In Eq. (1), V_{il}^γ is the hopping coefficient between the corresponding sites of the lead γ and of the central region. For simplicity, we take V_{il}^γ to be real and nonvanishing only if i,l are nearest neighbors. The last term in the Hamiltonian is written in terms of the on-site number operator $\hat{n}_l = a_l^\dagger a_l$ and describes the electron-electron interaction between charges localized in different sites of the central region. The interaction strength is characterized by the parameter U and r_l denotes the position of the lth site. t_L is the hopping energy on leads, $<,>$ denotes nearest neighbor summation and for simplicity the on-site energy of the leads is taken equal to zero.

Note that $\chi(t)$ switches both the coupling to the leads and the Coulomb interaction, which means that in our calculation, the initial correlations are neglected.[18,19] In the long-time limit when the system achieves a steady state, this approximation is permitted. Finally, t_{lm} are nearest neighbor hopping parameters inside the central region and the on-site energies ε_l may include a constant gate potential V_g.

The standard application of the Keldysh machinery leads to the following preliminary formula for the current through the lead α in the steady state of the system:

$$J_\alpha = \frac{e}{\pi\hbar} \sum_{i\in L_\alpha, m\in C} \int_{=\infty}^{\infty} dE\ \text{Re}[V_{mi}^\alpha G_{im}^<(E)], \tag{2}$$

where $G_{mi}^<(E)$ is the Fourier transform of the lesser Green function $G_{mi}^<(t,t') = i\langle a_i^\dagger(t) d_m(t)\rangle$. Note that the operators are written in the Heisenberg picture with respect to the total Hamiltonian and that we assumed the steady-state regime so that the Green function depends only on time differences. At this point, one has to express the mixed index Green function according to the Langreth rules,[18]

$$G_{li}^< = \sum_\gamma \sum_{j\in L_\gamma} \sum_{m\in C} (G_{lm}^R V_{mj}^\gamma g_{ji}^< + G_{lm}^< V_{mj}^\gamma g_{ji}^A), \tag{3}$$

where $g^{A,<}$ are the advanced and lesser Green functions of the semi-infinite leads that are known (see, for example, Ref. 44).

Substituting their expressions into Eq. (2), one ends up with the following (we omit the energy dependence for the simplicity of writing):

$$J_\alpha = \frac{ie}{\hbar} \int_{-2t_L}^{2t_L} dE\ \text{Tr}[\Gamma_\alpha (G^R - G^A) f_\alpha + G^<]. \tag{4}$$

In Eq. (4), the Green functions are to be understood as matrices and the trace means a sum over all sites of the central region. f_α is the Fermi function of the lead α and Γ^α is a matrix linewidth, which is essentially given by the density of states in the lead, $\rho(E) = \theta(|E| - 2t_L)\sqrt{4t_L^2 - E^2}/2t_L$, and by the hopping constant between the lead α and the central region [$\theta(x)$ is the step function],

$$\Gamma_{lm}^\alpha(E) = 2\pi V_{il}^\alpha V_{jm}^\alpha \rho(E). \tag{5}$$

Equation (4) was obtained for the first time by Jauho *et al.*[41] and has been widely used in transport calculations for both interacting and noninteracting structures. In the noninteracting case, the perturbation comes only from the coupling to the leads, whose self-energy is known,

$$\Sigma_{L,lm}^R(E) = V_{li}^\alpha V_{mj}^\alpha\ \text{Im}\ g_{ij}^R(E), \tag{6}$$

$$\Sigma_{L,lm}^<(E) = 2\pi i V_{li}^\alpha V_{mj}^\alpha g_{ij}^<(E). \tag{7}$$

When the Coulomb interaction is taken into account, the main technical task is to compute, within appropriate approximations, the interacting self-energy Σ_I that should then be plugged into the Dyson and Keldysh equations,

$$G^R = G_0^R + G_0^R(\Sigma_L^R + \Sigma_I^R)G^R, \tag{8}$$

$$G^< = G^R(\Sigma_L^< + \Sigma_I^<)G^A, \tag{9}$$

where $G_0^{R,<}$ are Green functions of the noninteracting disconnected system. Using the known identity (see Ref. 45) $G^R - G^A = 2iG^R\ \text{Im}(\Sigma_L^R + \Sigma_I^R)G^A$ and the Keldysh equation, one obtains

$$J_\alpha = \frac{e}{h} \int_{-2t_L}^{2t_L} dE\ \text{Tr}[\Gamma^\alpha G^R \Gamma^\beta G^A (f_\alpha - f_\beta) - \Gamma^\alpha G^R\ \text{Im}(\Sigma_I^< + 2f_\alpha \Sigma_I^R) G^A]. \tag{10}$$

This is an alternative form for the current that is particularly useful for emphasizing the limitations of the Landauer formula when applied to interacting systems.

One notices at once that the first term in the current has a Landauer form in spite of the fact that the Green functions appearing there are interacting quantities. The second term is given by the imaginary part of the interaction self-energy. In our previous work,[27] we used the above formula to investigate the controlled dephasing in single-dot Aharonov–Bohm interferometers Coulomb coupled to a charge detector. The self-energy was computed by a perturbative approach up to the second order in the interaction strength.

Here, we propose an alternative method to compute the interaction self-energy based on the random-phase approximation. The starting point of the RPA scheme is to construct the polarization operator Π. In the non-self-consistent version of the RPA that we implement here, the polarization operator is built from the noninteracting Green functions of

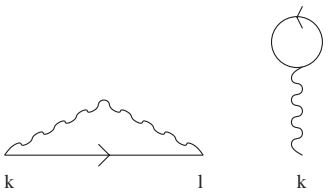

FIG. 1. The two types of diagrams contributing to the interaction self-energy. The solid lines represent noninteracting Green functions $G_{\rm eff}$ calculated in the presence of the leads and the wiggly line is the RPA potential.

the coupled system. We denote these functions by $G_{\rm eff}$ and compute them by the Dyson equation (in the Keldysh space) with respect to the self-energy of the leads,

$$G_{\rm eff} = G_0 + G_0 \Sigma_L G_{\rm eff}. \tag{11}$$

Since the Green functions we deal with are contour ordered, the polarization operator Π has also lesser and greater components, besides retarded and advanced ones (k,l are sites from the central region),

$$\Pi_{kl}(t_1,t_2) = -G_{{\rm eff},kl}(t_1,t_2) G_{{\rm eff},lk}(t_2,t_1). \tag{12}$$

Using the rules for diagrammatic expansion of the Keldysh–Green function, one is led to direct and exchange terms defined by the following RPA self-energies (the corresponding diagrams are given in Fig. 1):

$$\tilde{\Sigma}_{kl}(t_1,t_2) = iV_{kl}(t_1,t_2) G_{{\rm eff},kl}(t_1,t_2), \tag{13}$$

$$\tilde{\tilde{\Sigma}}_{kk}(t_1,t_2) = -i\sum_l V_{kl}(t_1,t_2) G_{{\rm eff},ll}(t_2,t_2), \tag{14}$$

where k,l denote sites from the central region and time arguments run along the two-branch Keldysh contour. V is the screened potential that obeys the Dyson equation with respect to the polarization operator Π,

$$V(t_1,t_2) = V_0(t_1,t_2) + \int dt \int dt' V_0(t_1,t)\Pi(t,t')V(t',t_2).$$

The above integrals are along the Keldysh contour and we introduced the instantaneous bare Coulomb potential,

$$V_{0,kl}(t,t_2) = \frac{U}{|r_k - r_l|}\delta_K(t_1 - t_2), \tag{15}$$

where the delta function is defined on the Keldysh contour (see, for example, Ref. 19),

$$\delta_K(t_1 - t_2) = \delta(t_1 - t_2)\tau_3, \quad \tau_3 = \begin{pmatrix} 1 & 0 \\ 0 & -1 \end{pmatrix}. \tag{16}$$

Note that on each branch of the Keldysh contour K, the Coulomb interaction is instantaneous and also that it does not couple different branches on the contour. Using again the Langreth rules, one obtains explicit expressions for lesser and retarded quantities while the integrals are to be performed on individual pieces of the Keldysh contour. The retarded polarization is computed via the Kramers–König relation and then the two basic equations for the polarization operator become

$$\Pi_{kl}^{<,>}(E) = -\frac{1}{2i}\int dE' G_{{\rm eff},kl}^{<,>}(E') G_{{\rm eff},lk}^{>,<}(E' - E), \tag{17}$$

$$\Pi^R(E) = \frac{i}{2\pi}\int dE' \frac{\Pi^>(E') - \Pi^<(E')}{E - E' + i0}. \tag{18}$$

Noticing that the integration range in Eq. (17) is restricted to $[-2t_L, 2t_L]$ and that Green function is nonvanishing only if $|E' - E| < 2t_L$, it follows that $E \in [-4t_L, 4t_L]$. At the next step, one has to compute the RPA interaction according to the Dyson and Keldysh equations,

$$V^R(E) = V_0 + V_0 \Pi^R(E) V^R(E), \tag{19}$$

$$V^{<,>}(E) = V^R(E)\Pi^{<,>}(E)V^A(E), \tag{20}$$

where in Eq. (20) we have used the property $V_0^< = 0$. The self-energies are then given by the following set of equations (the argument E covers the interval $[-2t_L, 2t_L]$, as required by the integral in the current formula):

$$\Sigma^{<,>}(E) = \tilde{\Sigma}^{<,>}(E) + \tilde{\tilde{\Sigma}}^{<,>}(E), \tag{21}$$

$$\tilde{\Sigma}_{kl}^{<,>}(E) = \frac{i}{2\pi}\int dE' V_{kl}^{>,<}(E') G_{{\rm eff},kl}^{<,>}(E - E'), \tag{22}$$

$$\tilde{\tilde{\Sigma}}_{kk}^{<,>}(E) = -\frac{i}{2\pi}\int dE' \sum_l G_{{\rm eff},ll}^{<,>}(E') V_{kl}^{>,<}(E), \tag{23}$$

$$\Sigma^R(E) = \frac{i}{2\pi}\int dE' \frac{\Sigma^>(E') - \Sigma^<(E')}{E - E' + i0}. \tag{24}$$

A particular feature of the RPA-Keldysh scheme is that the usual first order, direct, and exchange diagrams are not recovered when the RPA potential is introduced in the expressions for $\tilde{\Sigma}$ and $\tilde{\tilde{\Sigma}}$. The reason for this is the following: the self-energies contain the lesser and greater components $V^{<,>}$, which are given by the Keldysh equation whose first term is of order 2 in the bare Coulomb potential. This is different from the equilibrium version of RPA, wherein the self-energy contains the retarded component of the screened potential whose Dyson expansion starts with the first-order term. Therefore, we have to add by hand the first-order diagrams in the final result for the retarded self-energy,

$$\tilde{\Sigma}_{kl}^R(E) = \frac{i}{2\pi}\int dE' G_{{\rm eff},kl}^<(E - E') V_{0,kl}(E'), \tag{25}$$

$$\tilde{\tilde{\Sigma}}_{kk}^R(E) = -\frac{i}{2\pi}\int dE' \sum_{l\neq k} G_{{\rm eff},ll}^<(E') V_{0,kl}. \tag{26}$$

Equations (25) and (26) were obtained by again using the diagrammatic expansion and the Langreth rules. Note that in Eq. (26), the integrals are actually decoupled and that $\mathrm{Im}\,\tilde{\tilde{\Sigma}}_{kk}^R = 0$. Also, $\tilde{\Sigma}^R$ is off-diagonal because $V_{kk} = 0$ by defi-

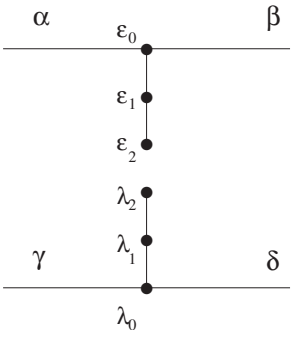

FIG. 2. Schematic of two T-shaped interferometers. The notations are explained in the text.

nition. Another useful quantity is the occupation number of the system, which is computed as usual from the lesser Green function (i runs over all sites of the quantum dot),

$$N = -\frac{i}{2\pi}\sum_i \int_{-2t_L}^{2t_L} dE G_{ii}^{<}(E) = \int_{-2t_L}^{2t_L} dE N(E), \qquad (27)$$

where $N(E)$ is the density of states.

We end this section with some comments about the expected range of validity for the RPA approach presented here. As pointed out by Henrickson *et al.*,[44] first-order self-consistent calculations break down when the interaction strength exceeds the hopping constant on leads. This is because in this range, elementary excitations are not captured by the perturbative approach. In a very recent work,[46] the density of states for interacting electrons in graphene was calculated within the RPA and no plasmonic excitations were reported. In the numerical simulations presented in Sec. III, the interaction strength is always much smaller than the hopping constant of the leads.

III. APPLICATION TO DEPHASING IN T-SHAPED INTERFEROMETERS

In this section, we use the above RPA-Keldysh scheme to study the transport properties of a quantum wire with a side-coupled quantum dot. The specific system we shall study is a one-dimensional quantum dot having two sites, one of which is coupled to a single channel lead. In order to compare the effects of interdot and intradot interactions, we consider also two such interferometers that are Coulomb coupled when placed close to one another (see the sketch in Fig. 2). The on-site energies of the dots are denoted by ε_m (upper interferometer) and λ_m (lower interferometer), $m=1,2$, and the hopping constant between the dots and the leads is denoted by τ. The sites of the leads where the dots are coupled are characterized by the on-site energy ε_0 and λ_0. The Hamiltonian of the system then reads as

$$H_{\rm cen} = \sum_{m=1,2} [(\varepsilon_m + V_g)a_m^\dagger a_m + (\lambda_m + V_g')b_m^\dagger b_m] + t_D(a_1^\dagger a_2 + b_1^\dagger b_2 + \text{H.c.}) + \tau(a_0^\dagger a_1 + b_0^\dagger b_1 + \text{H.c.})$$

$$H_{\rm int} = \frac{U}{2}\sum_{l,m,l\neq m} \frac{\hat{n}_l \hat{n}_m}{r_l - r_m}, \qquad (28)$$

$$H_{\rm tun} = t_L a_0^\dagger (d_{0\alpha} + d_{0\beta}) + t_L b_0^\dagger (d_{0\delta} + d_{0\gamma}) + \text{H.c.} \qquad (29)$$

The annihilation and creation operators for the upper and lower interferometer are denoted by $a_m, a_m^\dagger$ and $b_m, b_m^\dagger$. Also, we use the notations $a_0, a_0^\dagger$ and $b_0, b_0^\dagger$ for the operators associated with the two sites on the leads where the dots are attached. The hopping constant between the sites of the dots is t_D, while t_L is the hopping energy between the leads and the central region. 0ν, $\nu=\alpha,..,\gamma$ is the first site of the lead nu that is attached to the central region. We take $\varepsilon_m=\lambda_m$ to be the energy reference. V_g and V_g' simulate gate potentials applied on the dots. The last term in the Hamiltonian contains both the interdot and the intradot interactions between the two dots. $H_{\rm tun}$ is the tunneling term between the leads and the system. We can also include the interaction between the dot and the neighboring site of the lead but this is not essential for our discussion. The bias, the energy, the hopping constants on the leads, the coupling and interaction strengths, and the gate potential will be expressed in terms of the hopping energy t_D of the dots, which is chosen as the energy unit. The hopping energy on leads is $t_L=2t_D$, leading to a bandwidth of the leads $W=8t_D$ (recall that the spectrum of the semi-infinite one-dimensional lead is $[-2t_L, 2t_L]$). The numerical simulations were performed in the very low-temperature regime $kT=10^{-4}$.

A finite bias is applied on the leads, i.e., $V=\mu_\alpha-\mu_\beta$ and $V'=\mu_\gamma-\mu_\delta$, where $\mu_\alpha,\ldots,\mu_\delta$ are the chemical potential of the semi-infinite leads. We apply the bias in a symmetric way with respect to zero, that is, $\mu_{\alpha,\beta}=\pm V/2$ and $\mu_{\gamma,\delta}=\pm V'/2$. All the curves we present below were obtained by using a suitable grid for the energy range in the integrals in order to obtain stable results. Typically, one needs 1500 points in the range $[-4t_L:4t_L]$. The main care here is to take properly into account the very sharp peaks of the Green functions of the noninteracting system.

We first look at the role of the intradot interaction and consider only one interferometer. In Figs. 3(a) and 3(b), one finds the first and the second Fano line shapes of the current as a function of the gate potential V_g. The bias is fixed ($V=0.2$) and for the interaction strength we choose $U=0.1,0.2,0.3$. We present the two peaks in separate plots in order to better discern the dephasing effect. The Fano pattern of the current as a function of the gate potential applied on the lateral dot originates in the interference between electronic waves freely passing through the wire (forming the so-called background signal) and waves that are scattered at least once at the side-coupled dot (the resonant contribution). It is clear that in the interacting case, both the amplitude and the shape of the asymmetric Fano line change. A small reduction of the peak is seen but the main differences appear in the region of the Fano dip. At $U=0.1$, the dip is pushed above the noninteracting one, but it almost disappears at $U=0.2$. When further increasing the interaction to $U=0.3$, the first Fano dip is recovered and a local maximum develops on its left side. In contrast, the second dip is even more damaged. Below, we shall discuss these features in more detail. Figure 3(c) shows the density of states in the dot as a function of energy and gate potential in the case $U=0.2$. It is clear that at resonances (i.e., at $V_g\sim-1$ and $V_g\sim1$), the dot

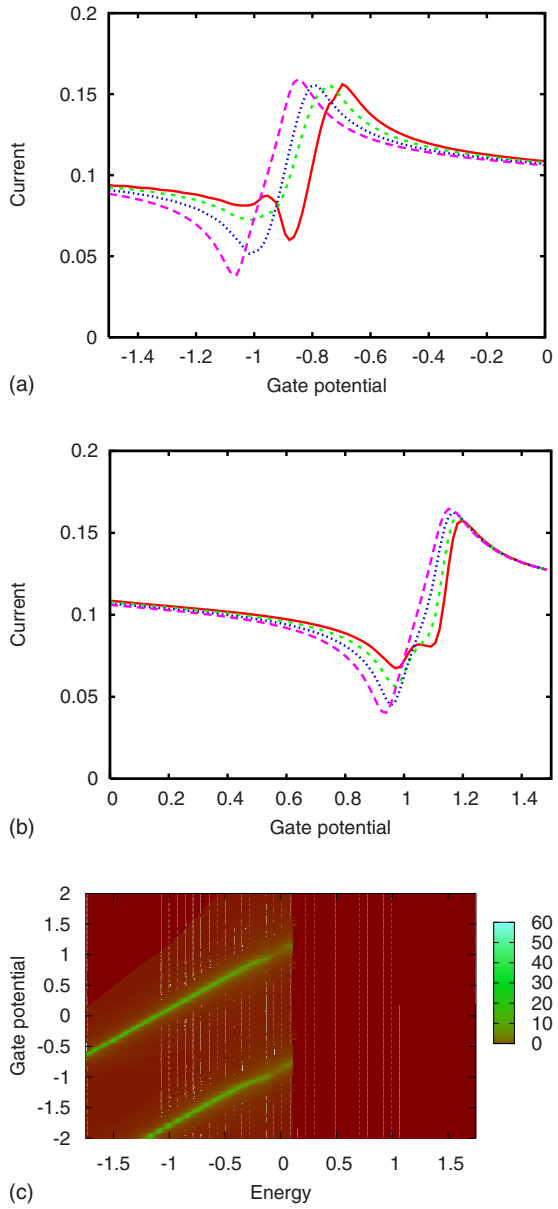

FIG. 3. (Color online) (a) The first and (b) the second Fano line shapes of the current through the interferometer as a function of the gate potential for different values of the interaction strength: full line, $U=0.3$; dashed line, $U=0.2$; dotted line, $U=0.1$; long-dashed line, $U=0.0$. (c) The density of states in the dot as a function of energy and gate potential (see the comments in the text). Other parameters: $V=0.2$, $\tau=0.35$, $\varepsilon=-0.75$, and $t_L=1$.

loses one electron as the localized states enter the bias window $[-0.1:0.1]$. This is why the two traces in Fig. 3(c) disappear at energies $E>0.1$. We have also performed numerical simulations for three- and four-site quantum dots and qualitatively obtained the same results.

We emphasize that a similar dephasing effect was obtained in our previous work,[27] but there the effect was entirely due to the Coulomb interaction between a single-site dot embedded in an Aharonov–Bohm ring and a nearby detector. Here, it is the intradot interaction that leads to decoherence.

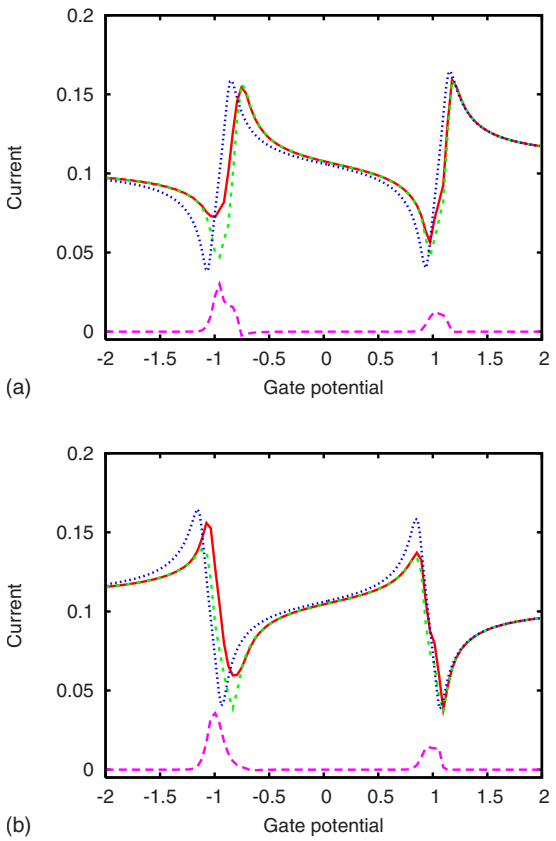

FIG. 4. (Color online) (a) The contribution of the two terms in the current formula for different signs of the Fano parameter (a) $q<0$ and (b) $q>0$. Full line, the total current; dashed line, the Landauer current J_c; long-dashed line, the correction J_i; dotted line, the noninteracting Fano line. Other parameters: $U=0.2$ $V=0.2$, $\tau=0.35$, and $t_L=1$.

We extend our analysis by showing in Figs. 4(a) and 4(b) the current through the interferometer for fixed bias $V=0.1$ and different signs of the Fano parameter. More precisely, the Fano parameter q is positive (i.e., the dip is located to the left side of the peak) if the on-site energy of the contact site $\varepsilon_0=-0.75$ and negative if $\varepsilon_0=0.75$. We plot also the separate contributions of each term in the current formula [Eq. (10)]. The second term gives just a "bump" around the Fano resonance and we shall denote this contribution by J_i as it is entirely due to the electron-electron interaction. The asymmetric shape of the resonance is given by the first term, which is proportional to the difference of the Fermi functions. Since in the noninteracting case this term is related to the Landauer formula for the conductance, we use the notation J_c.

In both Figs. 4(a) and 4(b), a reduction of the Fano line amplitude is noticed in the presence of electron-electron interaction. The line shapes move to the right, which is essentially due to a Hartree-type shift from the interaction self-energy. Another observation is that the second Fano resonance is less affected by the Coulomb interaction, its shift being also smaller than in the case of the first Fano line. This happens because there is more charge in the side-coupled quantum dot before the first resonant tunneling. It is well known that at resonance the occupation number N of the

dot decreases by 1 over a range that roughly equals the resonance linewidth. Now, clearly, the first Fano line corresponds to the transition $2 \rightarrow 1$ and the second one develops as the quantum dot is emptied i.e., $1 \rightarrow 0$ [see also the density of states given in Fig. 3(c)]. It is therefore understandable that the Coulomb effects are weaker on the second resonance.

The above comments apply to both Figs. 4(a) and 4(b). Now we discuss the details of dephasing. When $q<0$ [Fig. 4(a)], the suppression of the Fano line is mainly due to the enhanced value of the dip at $U=0.2$. The reason is evident when we look at the two contributions to the current. On one hand, J_c already displays a dip that is higher than the noninteracting one, and on the other hand, the correction J_i adds to the final value of the dip. Note that the Fano peaks are not drastically affected and that contribution of J_i decreases on the second resonance.

Turning to Fig. 4(b) in which $q>0$, we observe that the suppression of the first Fano interference is symmetric, in the sense that the dip is enhanced and the peak diminishes. It is also interesting to mention that the contribution due to J_i differently affects the two types of interference (constructive or destructive). In contrast to Fig. 4(a) where the maximum of J_i is located below the Fano dip, in Fig. 4(b) this point is rather below the Fano peak. As a consequence, the total peak is higher than J_c and the Fano dip is lower than the one in Fig. 4(a). Nevertheless, when comparing to the noninteracting Fano line, we see that a dephasing still exists. For the second line shape, the constructive interference (i.e., the Fano peak) is reduced and the destructive one is not changed. The correction is again present but it does not change either the peak or the dip and affects rather the middle of the Fano line.

The above discussion suggests that in the presence of an intradot interaction, both constructive and destructive Fano interference are affected and that their sensitivity depends on the sign of the Fano parameter, that is, on the order in which the two types of interference are experienced by the system. If $q<0$, the destructive interference appears first and the interaction effects are predominant. If $q>0$, the Fano peak amplitude reduces and the Fano dip is less affected.

Now, we discuss the behavior of the interaction self-energy, which will shed some light on the main processes that induce decoherence in the system. For this, we have to consider the various matrix elements of Σ_I.

In Fig. 5(a), we give the imaginary part of the retarded self-energy at the first site as a function of energy and gate potential [for a better visibility of Fig. 5(a), we actually plot $-\mathrm{Im}\,\Sigma_{I,11}$]. It is evident that at a very small temperature, it suffices to restrict the energy range to $[-0.1:0.1]$, which equals the bias window (we take $\mu_\alpha=0.1$ and $\mu_\beta=-0.1$). One observes that the main contribution to the imaginary part corresponds to gate potentials that are located around the two resonances. We remark that the maxima of the self-energy have rather equal heights but they are not aligned in energy. Actually, the maximum around the second resonance is not centered in the bias window. A similar behavior is obtained for $-\mathrm{Im}\,\Sigma_{I,22}$. The imaginary part of the off-diagonal element $\Sigma_{I,12}$ plotted in Fig. 5(b) is much smaller than the diagonal counterpart. This is expected because for long-range potentials, as it is the case here, the exchange diagrams can be

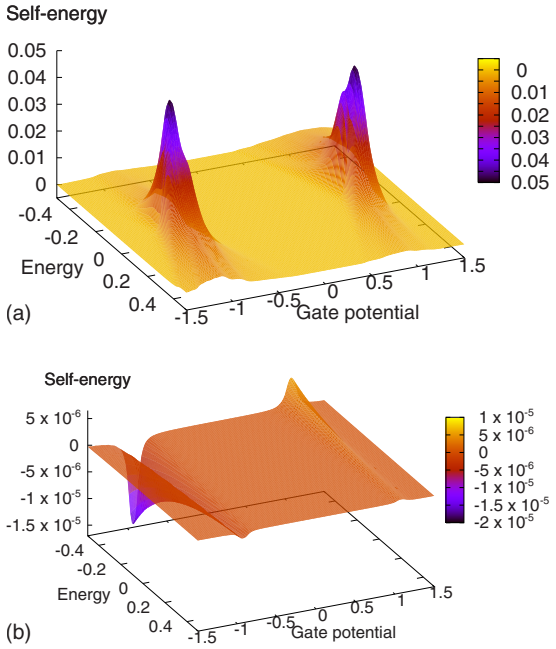

FIG. 5. (Color online) (a) $-\mathrm{Im}\,\Sigma^R_{I,11}$ as a function of energy and gate potential. The important contribution comes from energies inside the bias window $[-0.1:0,1]$ and for gate potentials at which the Fano resonances appear. (b) $\mathrm{Im}\,\Sigma^R_{I,12}$ as a function of energy and gate potential. Other parameters: $U=0.2$, $V_{sd}=0.2$, $\tau=0.35$, and $t_L=1$.

neglected with respect to the direct contribution.[47] Note that $\mathrm{Im}\,\Sigma_{I,12}$ is both positive and negative.

The imaginary part of the retarded self-energy is related to the inverse of the quasiparticle lifetime. In our case, there are two contributions to the resonance width: one comes from the leads' self-energy Σ^R_L and is roughly on the order of $\mathcal{O}(\tau)^2$ and the other one is entirely due to the Coulomb repulsion. From the diagrams that correspond to $\mathrm{Im}\,\Sigma_{I,11}$, it follows then that the dephasing in the upper interferometer, say, is mainly due to the interaction with at least one electron-hole pair that is excited in either one of the two subsystems. We recall that the creation and destruction of the electron-hole pairs are inelastic scattering processes.

In what concerns the real part of the interaction self-energy, it is responsible for the shift of the resonance and the main contribution is given by the Hartree diagram [see Eq. (26)]. This diagram contains the on-site occupation number that is constant except at resonance when electrons escape from the dot to the side-coupled leads. This behavior is easily checked in Fig. 6(a). Note that this term is energy independent since the involved scattering process is elastic. For completeness, we show in Fig. 6(b) the real part of the exchange self-energy $\Sigma_{I,12}$. Again, it is smaller than $\mathrm{Re}\,\Sigma_{I,22}$.

In the following, we investigate the transport properties of two identical T-shaped interferometers that are mutually coupled via the Coulomb interaction between the side-coupled dots. If not otherwise stated, all interactions (interdot and intradot) are taken into account. We take the same lead-dot coupling strength on both systems. When the interferometers have the same set of parameters, their Fano line shapes coincide. In Figs. 7(a) and 7(b), we compare the sec-

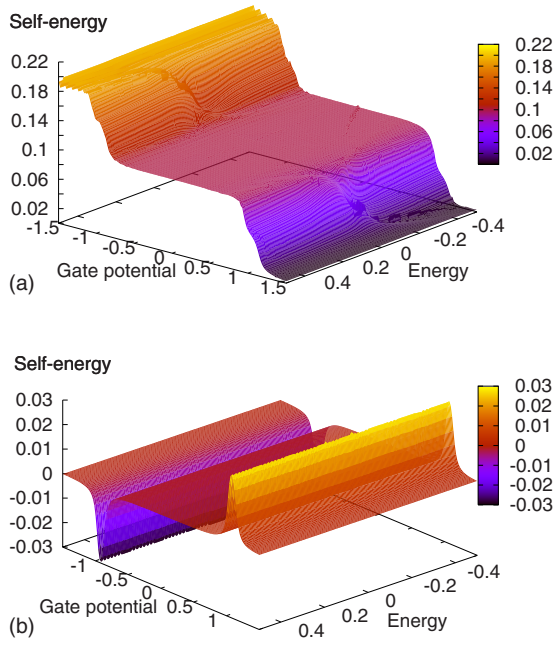

FIG. 6. (Color online) (a) Re $\Sigma^R_{l,11}$ and (b) Re $\Sigma^R_{l,12}$ as a function of energy and gate potential for the single interferometer. Other parameters: $U=0.2$, $V=0.2$, $\tau=0.35$, and $t_L=1$.

ond Fano resonance in this case to the similar curve from Figs. 4(a) and 4(b). The dephasing is now given by both intradot and interdot Coulomb interactions. Overall, the Fano lines are similar to the ones obtained for the single interferometer but several differences appear: (i) The Fano lines of the Coulomb-coupled interferometers are shifted even further to the right when compared to the single interferometer case. (ii) The constructive interference is more suppressed than in the single interferometer case. The reason for this is that when both systems are in the constructive regime, a large current passes through them and this amplifies the charge sensing effect.

It is a known fact, both experimentally and theoretically, that for two Coulomb-coupled systems, the dephasing effect increases at higher values of the bias.[13,27] We have checked this feature for the two T-shaped interferometers. Below, we present numerical results that emphasize a more interesting effect, namely, the enhancement of dephasing when *two* levels participate in the quantum interference, at a fixed and rather low bias. From the experimental point of view, this situation is met when bigger dots are used, which lead to a smaller level spacing, but also for double dots having a small interdot coupling. This is the situation we simulate in Figs. 8(a) and 8(b) by taking the hopping parameter between the two sites $t_D=0.25$ (the density of states in this case shows that there are two levels that enter the bias window when the gate potential is varied). We take $\varepsilon_0=-\lambda_0$ so that the two systems show line shapes with Fano parameters of different sign. Figure 8(a) shows the noninteracting Fano lines. Each system exhibits only one Fano line, and by comparing Fig. 8(a) to Fig. 7, one infers that in the two-level case, an additional shoulder appears in the middle of the Fano line. This is associated with the entrance of the second level inside the bias window. We notice that the amplitude of the resulting

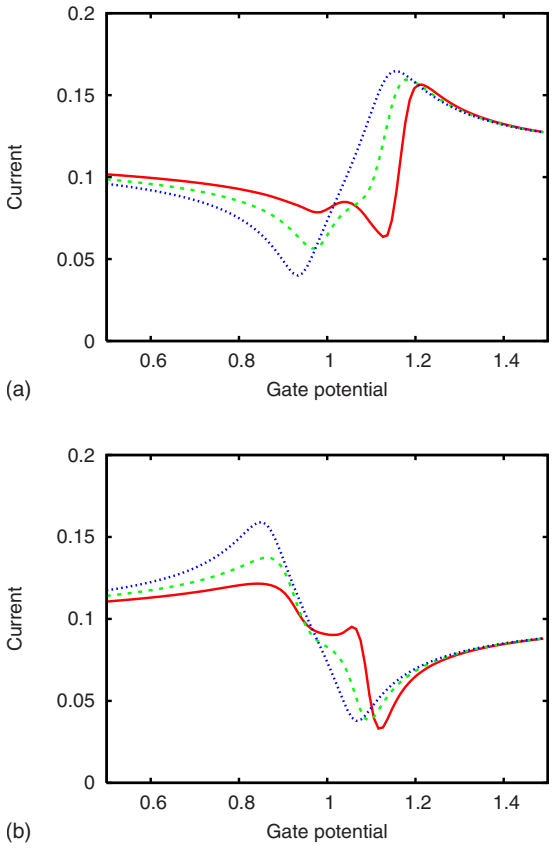

FIG. 7. (Color online) The cumulative effect of the interdot and intradot interaction can be noticed in the current through the upper interferometer (full line) when comparing to the current for a single interferometer (dashed line). The dotted line represents the noninteracting Fano line. The parameters are as in Fig. 4.

Fano line is not twice as large as the one shown in Fig. 7, which means that the contributions of the two levels to the current do no simply add. This suggests that a more complicated interference takes place in the system. Actually, each level causes an interference with the background signal, but the nature of this interference can be different (purely constructive, purely destructive, or intermediate). When electron-electron interactions are included in the calculation, a clear reduction of the constructive interference appears in the current through the lower interferometer. The additional shoulder is more difficult to discern. The upper interferometer shows, in turn, a Fano line whose dip is damaged. We believe that this dephasing effect for Coulomb-coupled T-shaped interferometers should be easily observed in experiments. One only has to compare the Fano line shapes of a single interferometer and of the double interferometer. Let us stress again that this effect does not require a large bias.

The analysis we made so far shows that both intradot and interdot Coulomb interactions cause a reduction in the Fano interference. Since the intradot interaction is bigger than the interdot repulsion, an important point would be to check if by placing a quantum dot near an interacting interferometer the controlled dephasing effects can still be discerned. To this end, we have performed numerical simulations for the interferometer with a two-site side-coupled dot, which is

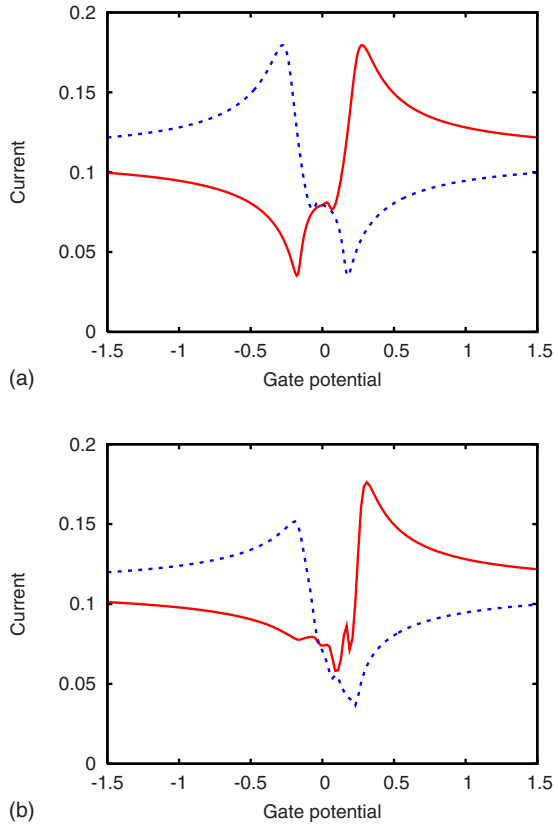

FIG. 8. (Color online) The two-level Fano effect for two T-shaped interferometers. By setting the hopping constant inside the dots to $t_D=0.25$, two levels can be brought inside the bias window of the leads by varying the gate potential. (a) Noninteracting case $U=0.0$ and (b) interacting case $U=0.2$. The bias is $V=V'=0.2$. The full line is the current through the upper interferometer; the dashed line represents the current through the lower interferometer.

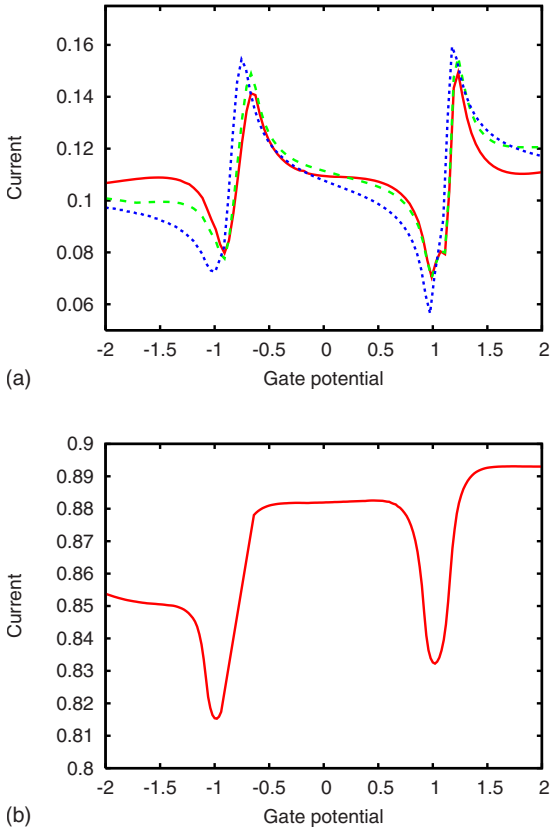

FIG. 9. (Color online) (a) The Fano interference in a T-shaped interferometer is further reduced when a nearby charge detector is subjected to a finite bias V'. Full line, $V'=2$; dashed line, $V'=1$. The dotted line represents the interacting Fano line in the absence of the detector. (b) The current across the detector as a function of the gate potential applied on the dot. The charge sensing effect leads to changes in the detector current around each Fano resonance in the side-coupled dot. Other parameters: $U=0.2$, $V=0.1$, $\tau=0.35$, and $t_L=1$.

Coulomb coupled to an additional single-site dot attached to biased leads. Due to the charge sensing effect, one expects to see changes in the current through the second dot when the Fano resonance develops in the interferometer. Conversely, the Fano line itself should be modified as the electrons are "detected" by the nearby quantum dot. In Fig. 9(a), we plot the current through the interferometer as a function of the gate potential for two values of the bias applied on the detector. For comparison, we also show the current in the absence of the detector (the dotted line). It is clear that at bias $V=1.0$, the amplitude of the Fano lines is reduced, both from the peak and the dip. We remark also that at $V=2.0$, it is only the Fano peak that decreases. Figure 9(b) confirms that the single-site quantum dot detects the passage of electrons through the side-coupled dot. Away from resonances, the current does not depend on V_g. This result suggests that controlled dephasing can be also put into evidence for T-shape interferometers.

One of the advantages of the Keldysh formalism is that it allows one to investigate the nonlinear transport regime, that is, to study the dependence of the current on the applied bias. We show in Fig. 10(a) the behavior of the current through a T-shaped structure with four side-coupled sites as a function of the applied bias for different values of the interdot interaction. The gate potential on the side-coupled sites is fixed to $V_g=0$ and also the on-site energy of the contact site is $\epsilon_0=0$. The bias was varied in a symmetric way as follows: we start with a negative bias $V=-4$ by choosing $\mu_\alpha=-2$ and $\mu_\beta=2$. Then, we simultaneously increase the chemical potential of the left lead and decrease the chemical potential of the right lead until the bias changes sign and reaches the final value $V=4$.

For $U=0$, the current displays the well-known steplike structure. The jumps between two steps correspond to a change in the number of states located inside the bias window. In the absence of the electron-electron interactions, the spectrum of the central region is symmetric with respect to zero. Consequently, the states whose energies differ just by a sign simultaneously align to the positive (negative) chemical potential of the leads, and at each passage between current steps, two more states enter or leave the bias window. In the interacting case, one notices the appearance of additional steps [see, for example, the step around $V=2$ shown in the inset of Fig. 10(a)]. This happens because the Coulomb interaction pushes up the spectrum breaking its symmetry and then two levels cannot enter or leave the bias window simul-

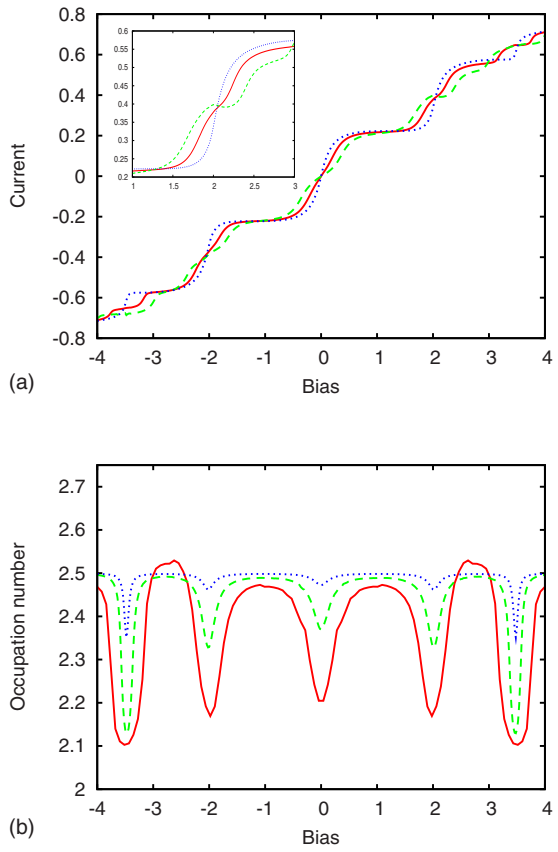

FIG. 10. (Color online) (a) Current vs bias for different interaction strengths: dotted line, $U=0$; full line, $U=0.15$; dashed line, $U=0.25$. The interaction leads to the formation of additional steps when compared to the noninteracting case. The inset shows the formation of a new step in the bias range [1:3]. (b) The occupation number of the dot as a function of bias for different interaction strengths. Full line, $U=0.15$; dashed line, $U=0.05$; dotted line, $U=0.01$. Other parameters: $\tau=1$ and $t_L=0.5$.

taneously. Clearly, the length of the steps increases with the interaction strength, a feature that was also noticed by Henrickson *et al.*[44] (see Fig. 5 of Ref. 44) within a self-consistent approach to nonlinear transport in interacting quantum dots. Note that the interaction does not affect the symmetry of the current curve with respect to the bias.

The dependence of the occupation number in the dot as a function of bias is shown in Fig. 10(b) and offers a better understating of the changes induced in the current curves by the Coulomb interaction. If the bias window covers the entire spectrum of the system, the occupation number $N\sim 2.5$, which corresponds to nearly half-filling. The highest energy level is the first one left *above* the bias window as the bias window shrinks, while the lowest energy level is still active for transport, as it is being pushed upward by the interaction. In this regime, the occupation number decreases. Then, the lowest level passes *below* the bias window and it can be fully occupied, which leads to an increase of the charge accumulated in the dot and a decrease in the current. Note that when the interaction increases and the bias $V=0$, the occupation number goes below 2.5 because the energy of the middle level is positive. We have also checked the current conservation (i.e., the identity $J_\alpha=-J_\beta$). The results presented above are consistent with previous self-consistent calculations of Henrickson *et al.*[44] and therefore show the reliability of our method. On the other hand, the RPA approach taken here is able to capture nontrivial effects due to the inelastic effects that cannot be reproduced by mean-field approximations.

We end with a discussion about the possible improvements of the present method. It is clear that one could perform self-consistent calculations by defining the polarization operator in terms of interacting Green functions. This procedure leads to longer times in the numerical simulations especially for large number of sites. Also, the self-consistency condition should be carefully checked at any value of the relevant parameters (interaction strength or the tunneling constant between the dot and the lead). In the self-consistent scheme, the self-energies will be directly related to the interacting Green functions and the position of the poles is expected to be slightly different from the noninteracting case due to the Hartree shift. Nevertheless, for the few-level system we are considering here, this does not lead to qualitative changes in the numerical results.

IV. CONCLUSIONS

We have implemented the random-phase approximation in the framework of the nonequilibrium Keldysh Green's function formulation for electronic transport in many-level quantum dots. The starting point is the polarization operator, which in the present approach is built from noninteracting Green functions. The calculation of interaction self-energy takes into account all scattering processes that involve electron-hole pairs and also the contribution of the exchange diagram. This approach has therefore a clear advantage over the second-order perturbation theory in the interaction strength used previously in Ref. 27 and could also be used as an alternative to the equation-of-motion approach or to the mean-field approximation.

As a first application of this method, we have considered the interplay between the intradot and interdot interactions in electronic transport in Coulomb-coupled T-shaped interferometers. For a single interferometer, the numerical calculations show that the intradot electron-electron interaction itself suppresses the quantum interference, even in the low bias regime. The various contributions to the interaction self-energy were analyzed as well as the dependence on the bias and gate potential.

In the presence of a second T-shaped interferometer or of a charge detector coupled to leads, further dephasing appears due to the charge sensing effect. We show that the dephasing increases when the Fano interference implies two levels of the dot, which are coupled to the continuum. The high tunability of side-coupled quantum dots should allow the observation of our theoretical predictions in future experiments.

ACKNOWLEDGMENTS

V.M. acknowledges financial support by TUBITAK-BIDEB and by CEEX Grant No. D11-45/2005. B.T. is supported by TUBITAK (Grant No. 106T052) and TUBA.

[1] Y. Imry, *Introduction to Mesoscopic Physics* (Oxford University Press, Oxford, 2002).
[2] *Semiconductor Spintronics and Quantum Computation*, edited by D. D. Awschalom, D. Loss, and N. Samarth (Springer, Berlin, 2002).
[3] R. I. Shechter, Zh. Eksp. Teor. Fiz. **63**, 1410 (1972) [Sov. Phys. JETP **36**, 747 (1973)].
[4] E. Ben-Jacob and Y. Gefen, Phys. Lett. **108A**, 289 (1985).
[5] D. V. Averin and K. K. Likharev, J. Low Temp. Phys. **62**, 345 (1986).
[6] H. van Houten, C. W. J. Beenakker, and A. A. M. Staring, in *Single Charge Tunneling*, NATO Advanced Studies Institutes, Series B: Physics Vol. 294, edited by H. Grabert and M. H. Devoret (Plenum, New York, 1992).
[7] D. Goldhaber-Gordon, H. Shtrikman, D. Mahalu, D. Abusch-Magder, U. Meirav, and M. Kastner, Nature (London) **391**, 156 (1998).
[8] M. Field, C. G. Smith, M. Pepper, D. A. Ritchie, J. E. F. Frost, G. A. C. Jones, and D. G. Hasko, Phys. Rev. Lett. **70**, 1311 (1993).
[9] A. C. Johnson, C. M. Marcus, M. P. Hanson, and A. C. Gossard, Phys. Rev. Lett. **93**, 106803 (2004).
[10] B. L. Altshuler, A. G. Aronov, and D. E. Khmelnitskii, J. Phys. C **15**, 7367 (1982).
[11] A. Stern, Y. Aharonov, and Y. Imry, Phys. Rev. A **41**, 3436 (1990).
[12] S. A. Gurvitz, arXiv:quant-ph/9607029 (unpublished); Phys. Rev. B **57**, 6602 (1998).
[13] E. Buks, R. Schuster, M. Heiblum, D. Mahalu, and V. Umansky, Nature (London) **391**, 871 (1998).
[14] T. Fujisawa, D. G. Austing, Y. Tokura, Y. Hirayama, and S. Tarucha, J. Phys.: Condens. Matter **15**, R1395 (2003).
[15] U. Sivan, Y. Imry, and A. G. Aronov, Europhys. Lett. **28**, 115 (1994).
[16] B. L. Altshuler, Y. Gefen, A. Kamenev, and L. S. Levitov, Phys. Rev. Lett. **78**, 2803 (1997).
[17] C. Caroli, R. Combescot, P. Nozieres, and D. Saint-James, J. Phys. C **4**, 916 (1971).
[18] H. Haug and A.-P. Jauho, *Quantum Kinetics in Transport and Optics of Semiconductors* (Springer, Berlin, 1996).
[19] M. Wagner, Phys. Rev. B **44**, 6104 (1991).
[20] D. N. Zubarev, Sov. Phys. Usp. **3**, 320 (1960).
[21] C. Lacroix, J. Phys. F: Met. Phys. **11**, 2389 (1981).
[22] V. Kashcheyevs, A. Aharony, and O. Entin-Wohlman, Phys. Rev. B **73**, 125338 (2006).
[23] Y. Meir, N. S. Wingreen, and P. A. Lee, Phys. Rev. Lett. **66**, 3048 (1991).
[24] B. R. Bulka and P. Stefanski, Phys. Rev. Lett. **86**, 5128 (2001).
[25] I. V. Dinu, M. Ţolea, and A. Aldea, Phys. Rev. B **76**, 113302 (2007).
[26] A. Silva and S. Levit, Phys. Rev. B **63**, 201309(R) (2001).
[27] V. Moldoveanu, M. Ţolea, and B. Tanatar, Phys. Rev. B **75**, 045309 (2007).
[28] J. König, Y. Gefen, and A. Silva, Phys. Rev. Lett. **94**, 179701 (2005).
[29] S. V. Faleev and M. I. Stockman, Phys. Rev. B **66**, 085318 (2002); **62**, 16707 (2000).
[30] U. Wulf, P. N. Racec, and E. R. Racec, Phys. Rev. B **75**, 075320 (2007).
[31] K. Kobayashi, H. Aikawa, A. Sano, S. Katsumoto, and Y. Iye, Phys. Rev. B **70**, 035319 (2004).
[32] G. Hackenbroich, W. D. Heiss, and H. A. Weidenmüller, Phys. Rev. Lett. **79**, 127 (1997).
[33] R. Berkovits, F. von Oppen, and Y. Gefen, Phys. Rev. Lett. **94**, 076802 (2005).
[34] M. Sato, H. Aikawa, K. Kobayashi, S. Katsumoto, and Y. Iye, Phys. Rev. Lett. **95**, 066801 (2005).
[35] Tae-Suk Kim and S. Hershfield, Phys. Rev. B **63**, 245326 (2001).
[36] R. Franco, M. S. Figueira, and E. V. Anda, Phys. Rev. B **67**, 155301 (2003).
[37] P. S. Cornaglia and D. R. Grempel, Phys. Rev. B **71**, 075305 (2005).
[38] P. A. Orellana, F. Dominguez-Adame, I. Gómez, and M. L. Ladrón de Guevara, Phys. Rev. B **67**, 085321 (2003).
[39] J. König and Y. Gefen, Phys. Rev. Lett. **86**, 3855 (2001).
[40] A. Silva and S. Levit, Europhys. Lett. **62**, 103 (2003).
[41] A.-P. Jauho, N. S. Wingreen, and Y. Meir, Phys. Rev. B **50**, 5528 (1994).
[42] H. D. Cornean, H. Neidhardt, and V. A. Zagrebnov, arXiv:0708.3931 (unpublished).
[43] V. Moldoveanu, V. Gudmundsson, and A. Manolescu, Phys. Rev. B **76**, 085330 (2007).
[44] L. E. Henrickson, A. J. Glick, G. W. Bryant, and D. F. Barbe, Phys. Rev. B **50**, 4482 (1994).
[45] H. M. Pastawski, L. E. F. Foa Torres, and E. Medina, Chem. Phys. **281**, 257 (2002).
[46] Xin-Zhong Yan and C. S. Ting, Phys. Rev. B **76**, 155401 (2007).
[47] A. L. Fetter and J. D. Walecka, *Quantum Theory of Many-Particle Systems* (McGraw-Hill, New York, 1971).